Device

Article

Modular tactile sensing platform with sequential optical sampling for human-robot interfaces

Graphical abstract

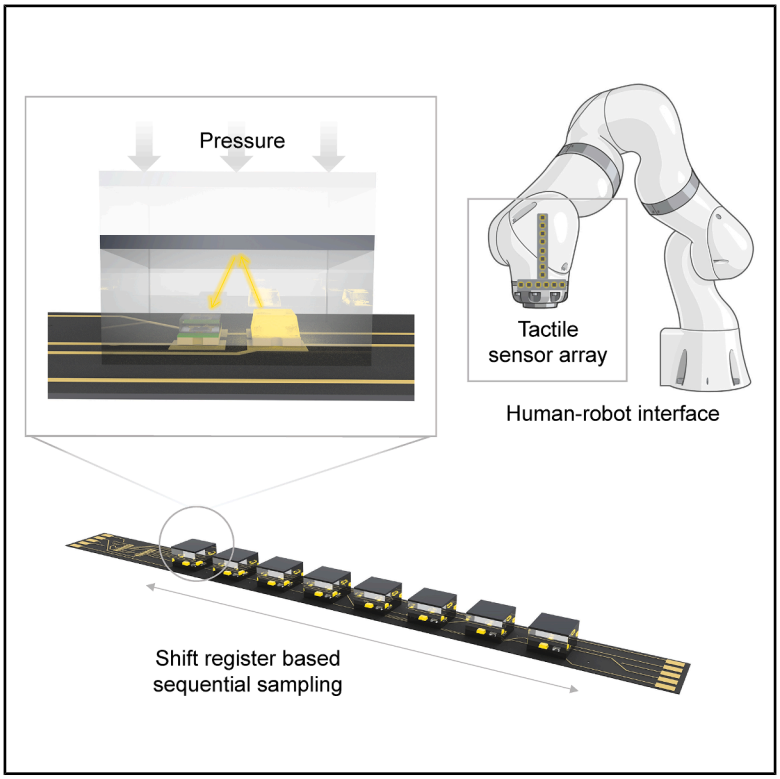

Authors

Hyunjin Kim (김현진), Seokjoo Cho (조석주), Chankyu Han (한찬규), ..., Yongrok Jeong (정용록), Jungrak Choi (최중락), Inkyu Park (박인규)

Correspondence

inkyu@kaist.ac.kr (I.P.), cjr1992@etri.re.kr (J.C.)

In brief

Kim et al. present a modular tactile sensing platform that combines optical multiplexing with deep learning to extend tactile perception resolution beyond sensor density. The system employs fixed wiring and sequential optical sampling to support scalable large-area tactile interfaces for human-robot interaction and wearable robotic systems.

Highlights

- Modular tactile sensor platform has been developed with sequential optical sampling
- Deep learning-based super-resolution for sparse tactile measurements
- Scalable tactile sensing without increased wiring or circuit complexity
- Enhanced human-robot interaction through high-resolution tactile mapping

3 Develop
Prototype with demonstrated applications in relevant environment

Kim et al., 2026, Device *4*, 101081

https://doi.org/10.1016/j.device.2026.101081

CellPress

Please cite this article in press as: Kim et al., Modular tactile sensing platform with sequential optical sampling for human-robot interfaces, Device (2026), https://doi.org/10.1016/j.device.2026.101081

Device

CellPress

Article

Modular tactile sensing platform with sequential optical sampling for human-robot interfaces

Hyunjin Kim (김현진),[1,7] Seokjoo Cho (조석주),[1,7] Chankyu Han (한찬규),[1] Jihyeon Ahn (안지현),[1,2] Donho Lee (이돈호),[1] Seungtaek Jang (장승택),[1] Gihun Lee (이기훈),[1] Kichul Lee (이기철),[1] Hyeonseok Han (한현석),[1] Ji-Hwan Ha (하지환),[3] Junseong Ahn (안준성),[4] Yongrok Jeong (정용록),[5] Jungrak Choi (최중락),[1,6,*] and Inkyu Park (박인규)[1,8,*]

[1]Department of Mechanical Engineering, Korea Advanced Institute of Science and Technology, Daejeon 34141, Republic of Korea
[2]Korea Institute of Machinery and Materials (KIMM), Daejeon 34103, Republic of Korea
[3]Department of Mechanical Engineering, Hanbat National University, Yuseong-gu, Daejeon 34158, Republic of Korea
[4]Department of Control and Instrumentation Engineering, Korea University, Sejong 30019, Republic of Korea
[5]School of Mechanical Engineering, Kyungpook National University, Daegu 41566, Republic of Korea
[6]Electronics and Telecommunications Research Institute (ETRI), Daejeon 34129, Republic of Korea
[7]These authors contributed equally
[8]Lead contact
*Correspondence: inkyu@kaist.ac.kr (I.P.), cjr1992@etri.re.kr (J.C.)
https://doi.org/10.1016/j.device.2026.101081

THE BIGGER PICTURE Tactile perception is essential for safe robot interaction with humans and complex environments, particularly as emerging healthcare and wearable systems require large-area, conformable tactile interfaces. However, scaling tactile systems remains challenging, as increasing sensor density is often accompanied by greater wiring complexity, bulky electronics, and limited reconfigurability, hindering practical deployment. Modular tactile systems have been proposed to improve flexibility and reconfigurability, but many still rely on complex electrical interconnections that constrain scalability. Addressing these limitations requires a system-level design shift. To bridge this gap, we present a modular tactile platform based on sequential optical sampling that decouples hardware complexity from sensor scalability. Combined with machine learning-enhanced super-resolution, this approach provides a customizable and practical solution for next-generation human-robot interfaces.

SUMMARY

Tactile sensors are essential for physical human-machine interaction, but array architectures are limited in scalability, wiring complexity, and adaptability to nonuniform surfaces. Here, we present a modular tactile sensor platform based on sequential optical sampling that enables scalable signal acquisition from arbitrarily arranged sensor modules using a fixed number of electrical connections. Each module integrates a light-emitting diode (LED) and a photodiode (PD) within a unified optical readout scheme. The system supports pressure mapping over a 0–100 kPa range with a 0.15 s response time, plug-and-play reconfiguration, and miniaturization down to 4 × 4 mm per module. A machine learning-assisted force localization approach achieved a spatial resolution of 2.5 mm with a mean prediction error of 16.0 mN. Robotic integration demonstrated contact detection and safety-triggered control.

INTRODUCTION

Tactile sensors allow machines to detect and respond to physical contact, providing feedback in tasks that involve manipulation, interaction, or safety.[1–3] As robotics continue to expand into healthcare, manufacturing, and consumer environments, there is an increasing need for scalable, reconfigurable, and conformable tactile sensors.[4–6] Conventional readout strategies, such as discrete wiring and row-column addressing, face severe scalability bottlenecks due to increasing wiring complexity and the requisite bulkiness of multi-channel circuit boards.[7–9] These constraints are particularly critical in conformable applications, where excessive interconnects on curved geometries exacerbate integration difficulties and the risk of mechanical entanglement or failure.

To overcome these challenges, researchers have explored modularization strategies in tactile sensor design. Module-level integration of microcontrollers and analog-to-digital converters has been proposed to support distributed processing and flexible layouts.[10–12] Such approaches lead to high power

Please cite this article in press as: Kim et al., Modular tactile sensing platform with sequential optical sampling for human-robot interfaces, Device (2026), https://doi.org/10.1016/j.device.2026.101081

consumption and increased cost due to duplicated electronics. Event-based spike sensing has been introduced as an energy-efficient readout strategy that generates potential spikes only when dynamic forces occur. While this principle enables low-power operation through event-based sensing with a fixed number of wirings, it lacks the capability to detect static loads.[13] Frequency domain encoding enables signal distinction through resonant frequencies but suffers from spectral interference and requires per array recalibration.[5,7] Machine learning-assisted identification based on shape-induced response variation can improve performance, but it requires more training data, as the number of sensor modules increases.[2,14] These prior methods show practical limitations in power consumption, sensing capability under static and dynamic loading, calibration complexity for individual sensors, and recalibration requirements for each array. It is necessary to develop a modularized sensor that can be customized into various array configurations while maintaining a fixed number of connections between the sensor array and the central controller, overcoming the remaining limitations. To clarify the distinctions among existing modular and optical tactile sensing strategies, a comparative summary of representative approaches—including discrete, multiplexer-based, electrical impedance tomography (EIT), frequency domain, and machine learning-based methods—is provided in Table S1.

In this work, we present a modular tactile sensor platform based on a shift register-based sequential optical sampling (SRSOS) method. Using shift registers,[15,16] where digital data cascade sequentially through a chain of flip-flops triggered by a clock signal, this approach enables pressure data acquisition from a large number of sensor modules through a compact set of control and readout lines. By sequentially activating each light-emitting diode (LED) via a shared clock and data input and reading photodiode signals through a common analog output, the number of physical connections to the central circuit remains constant regardless of the array size. This architecture eliminates the need for individual-addressing or complex routing, simplifying integration and enhancing scalability. Each module integrates a light-emitting diode (LED), a photodiode (PD), and a soft reflective layer and is electrically and mechanically independent. In this architecture, the central circuit board remains compact and fixed in size, while the number and arrangement of sensor modules can be freely customized. By sequentially activating each LED and reading the PD signal through a shared analog channel, the system performs time-multiplexed sensing without requiring individual wiring for each module. The modular design supports cost-effective and user-friendly reconfiguration of tactile sensor arrays. Sensors can be flexibly arranged to match arbitrary geometries, and modules can be reused or replaced without changes to the central circuit. This platform supports plug-and-play functionality, on demand scalability, and mechanical adaptability, with miniaturization down to 4×4 mm per sensing pixel. We demonstrate that the system maintains stable performance across varying mechanical loads, ambient lighting conditions, and array configurations. Machine learning-based signal processing enhances the spatial resolution 10-fold, enabling force localization at 2.5 mm intervals without increasing sensor density. The system also provides real-time visual feedback, allowing intuitive monitoring of tactile information through pressure-dependent color or brightness modulation. The system is validated through integration with a collaborative robotic arm, where it enables real-time feedback and safety-based interaction, highlighting its potential as a tactile interface for human-machine integration.

RESULTS AND DISCUSSION

Sequential optical sampling for scalable tactile sensing

The system concept illustrates a modular tactile platform that employs serial sensor connections and sequential optical sampling to enable flexible array configurations while minimizing structural and circuit complexity (Figure 1A). Signal acquisition is streamlined via time-multiplexed sampling, and the modular architecture ensures signal integrity without crosstalk, even in multi-sensor configurations. The concept is validated through real-time visual feedback under varying pressure inputs and physical interaction with robotic systems, supporting its use in human-machine interface applications. Each sensor module integrates an LED, a PD, and a compressible elastomeric layer with a reflective surface (Figure 1B). Pressure-induced compression reduces the distance between the LED and PD, increasing reflected light intensity and thereby the PD current, which is then converted into voltage via a transimpedance amplifier (TIA), where the PD is operated in photovoltaic mode to minimize dark current (Figure 1C).

The system architecture comprises a central measurement circuit and an expandable sensor array (Figure 1D). Each module includes a control block that receives a global clock and data input (Figure 1E). Sequential sampling is achieved via a shift register, activating one LED at a time while maintaining a fixed number of input/output (I/O) lines. All PDs are connected in parallel to form a single PD output channel, which is fed into the inverting input of the TIA circuit. All PD outputs are combined and read through a single PD_{output} analog channel, enabling system operation using five wires: power, ground, data input, PD output, and clock. The modular architecture ensures spatial separation between sensing elements, while the measured voltage variation is primarily governed by the compression-induced change in the optical path length between the LED, reflective surface, and PD. This process corresponds to the SRSOS method. A signal model is provided in Equation 1. In Equation 1, V_{IN} is the output voltage of the TIA, $I_d$is the photocurrent, the d' *thPD* when its d' *thLED* is activated, R_f is the feedback resistor in the TIA circuit, and $f(Pressure_d)$ denotes the relationship between the applied pressure on the d' *th* module and the resulting sensor response:

$$V_{IN} = (I_1 + I_2 + \ldots + I_d + \ldots + I_{m-1} + I_m) * R_f$$

$$\approx I_d * R_f \approx f(Pressure_d) \text{ when } d'\text{th LED is on}. \quad \text{(Equation 1)}$$

Based on the SRSOS mechanism, the modules can be fabricated individually and conveniently interconnected to expand the array size. Figure 1F demonstrates the plug-and-play capability, where arrays can be reconfigured in real time without additional fabrication. The sequential activation of LEDs based on shift register control is illustrated in a timing diagram (Figure 1G), where each rising clock edge advances the data

Please cite this article in press as: Kim et al., Modular tactile sensing platform with sequential optical sampling for human-robot interfaces, Device (2026), https://doi.org/10.1016/j.device.2026.101081

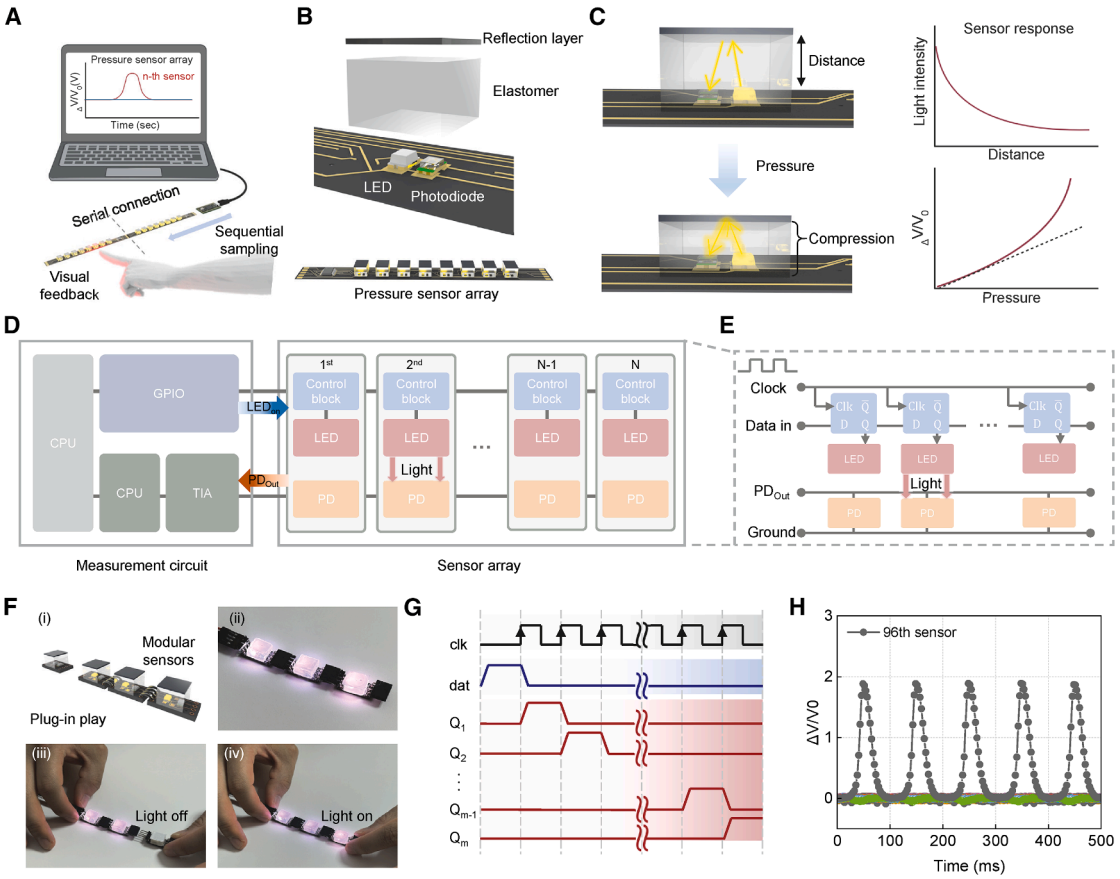

Figure 1. Overview of the modular optical tactile sensor system and measurement architecture

(A) Schematic of the modular pressure sensor array with sequential sampling and visual feedback.

(B) Exploded view of a single sensor module consisting of a light-emitting diode (LED), a photodiode (PD), and a compressible elastomer with a reflective layer.

(C) Working principle of the optical pressure-sensing mechanism.

(D) System diagram of the measurement circuit and sensor array.

(E) Diagram of shift register-based control using shared clock and data lines.

(F) Schematic and photograph of the proposed optical tactile sensor module with plug-and-play capability.

(G) Timing diagram of LED activation using shift register logic.

(H) Vibration input to the 96th sensor without crosstalk.

stream to trigger the next LED. This simplified control scheme reduces overhead compared to conventional row-column scanning approaches. The control is implemented using cascaded D-type flip-flops, where each rising clock edge propagates one bit, sequentially triggering LED activation (Figures S1A and S1B). Based on this mechanism, the system supports scalable operation across large arrays. As the number of connected LEDs increases, the control frequency decreases, as characterized across up to 1,000 modules (Figure S1C). Sampling rates were characterized from 100 to 1,000 sensors, yielding consistent operation with frequencies ranging from 380 Hz down to 38 Hz (Figure S1D). This decrease originates from the sequential readout architecture and represents a typical trade-off between spatial resolution and temporal bandwidth in multiplexed systems. Higher frame rates can be achieved by employing multiple analog-to-digital converter (ADC) channels or faster converters, depending on the application requirements.

The power consumption of the system was characterized across different operating clock speeds. The sensor modules consumed 50 mW regardless of the number of connected units due to sequential LED operation. System-level consumption, including the microcontroller, ranged from 0.15 to 0.50 W depending on the clock frequency (Figure S2). The voltage drop across the sensor array was measured to evaluate signal consistency under extended wiring. A 0.83% decrease (from 3.26 to 3.23 V) was observed across 96 LEDs, with negligible effect on brightness uniformity (Figure S3). This minor reduction originates primarily from the finite resistance of the prototype wiring and does not represent an intrinsic limitation of the proposed architecture. In practice, thicker or lower-resistance power lines can suppress such a voltage drop even for larger arrays, while any residual offset can be compensated during initial calibration. Because only one LED-PD pair is sequentially activated at any given time, the effective electrical loading does not accumulate

Please cite this article in press as: Kim et al., Modular tactile sensing platform with sequential optical sampling for human-robot interfaces, Device (2026), https://doi.org/10.1016/j.device.2026.101081

with increasing array size and remains stable, with variation below 1%, as inferred from the voltage drop measurement, ensuring scalable power distribution.

The timing response of the electronics was evaluated by introducing controlled delays between LED activation and signal acquisition. A symmetric readout sequence was implemented, where the PD signal was sampled during both LED-on and LED-off periods to differentiate sensing from ambient light (Figure S4A; Video S1). Identical voltage levels were observed under both slow (5 Hz) and fast (28 kHz) driving conditions, indicating stable behavior across the full range of sampling speeds (Figure S4B). The maximum reliable sampling rate was determined to be ~28 kHz, corresponding to an ADC conversion time of ~36 μs. This hardware ceiling at approximately 28 kHz was imposed by the ADC conversion time and the propagation speed of the shift register. As these are not intrinsic to the sensing mechanism, higher sampling rates can be achieved by employing faster ADCs and shift control circuits. To evaluate signal independence, a 10 Hz vibration input was applied to the 96th sensor in a tactile sensor array (Figure S5). The vibration pattern appeared only in the signal from corresponding module, while signals from neighboring modules remained unchanged, confirming the absence of crosstalk and validating the signal isolation capabilities of the optical readout system (Figure 1H).

Tactile sensor design and performance evaluation

The performance of the modular pressure sensor was evaluated through a series of experiments designed to assess sensitivity, scalability, signal repeatability, and plug-and-play functionality (Figure 2). Each pressure sensor module consists of an LED-PD pair embedded beneath a compressible elastomer and a thin reflective layer, as previously described (Figures 1B and 1C). Fabrication involved a multi-step molding process, including elastomer pouring, dye or particle integration, and spin coating of the reflective surface (Figure S6A). The reflective layer had a thickness of approximately 0.7 mm. A photograph of the completed module is shown in Figure S6B. To assess signal isolation, three sensor modules were sequentially loaded with 40, 50, and 80 kPa pressure (Figure 2A). Each module exhibited a distinct and isolated voltage change, with no interference observed in the other modules. Only the targeted module exhibited a voltage change, while others remained inactive, confirming signal isolation. This response was validated in separate trials where pressure was applied to only the second or third module (Figure S7). Under cyclic loading conditions, consistent signal patterns were observed across all three modules, demonstrating stable and synchronized behavior in a multi-module configuration (Figure 2B). Additionally, the output remained consistent regardless of whether pressure was applied to a single module or multiple modules simultaneously, validating the independence and robustness of the readout mechanism (Figure 2C).

The scalability of the platform was assessed by increasing the number of connected modules up to 25 and comparing the resulting sensor responses. For each configuration, a step load of 160 kPa was applied only to the last module, while the other connected modules remained unloaded. Under a step loading of 160 kPa, the sensor maintained a rise time of approximately 15 ms regardless of the number of modules (Figure 2D). The sensor output remained consistent up to 100 kPa across all configurations, indicating that module expansion does not affect sensitivity or calibration characteristics (Figure 2E). In addition, material selection of the reflective layer was optimized to improve response uniformity. A series of experiments confirmed that reflectivity increased with dye concentration but saturated beyond 5%, which was adopted as the standard for sensor fabrication (Figure S8). Mechanical reliability was validated through 1,000-cycle pressure loading tests at 150 kPa. The sensor demonstrated repeatability with minimal drift across all cycles (Figure 2F).

The system supports plug-and-play operation without reconfiguration, as demonstrated in Figure 1F. Each module integrates electrical and mechanical connectors, enabling real-time recognition upon addition or removal. When a module is connected, the corresponding control signal activates its embedded LED, and the emitted light is detected by the paired PD within the same module, generating a voltage output. This output is compared against a predefined threshold voltage of 500 mV. Activation of the LED results in a PD response that exceeds this threshold, confirming the presence of the newly attached module. In contrast, if the module is absent or has been disconnected, then the same control signal cannot trigger LED emission, and, consequently, the PD output remains below the threshold level. This difference in the PD response provides a robust function of real-time detection for both connection and disconnection events. This behavior is demonstrated in Figures 2G and 2H and Video S2, where real-time detection of modules 2 and 3 was achieved.

To ensure operation under varying lighting conditions, the system utilizes the sequential LED control mechanism of the shift register architecture (Figure 2I). During normal operation, a logical "1" is shifted through the register to sequentially activate one LED at a time. When no LED is active (i.e., the "1" has passed through all modules), then the system enters an all-off state. The signal acquired at this point is defined as the reference voltage V_{ref}, representing the ambient light condition. For each module, the calibrated pressure signal is computed as $V_{cal} = V_{on} - V_{ref}$, where V_{on} is the signal when the module's LED is active. This reference stabilizes the sensor baseline and enables reliable pressure detection even under changing illumination, as demonstrated in Figures 2J and Video S1. The proximity sensitivity test was conducted to verify that non-contact proximity does not interfere with the tactile response of the sensor. The proximity sensitivity of the sensor was evaluated by observing signal changes as a reflective object approached the surface without contact. White dye resulted in a 17.2% signal increase due to proximity, while metallic particles showed only a 1.36% change (Figure S9). Reflective layers incorporating white dye exhibit higher optical transmittance, making them more responsive to proximity effects compared to metallic layers. Although higher transmittance increases proximity sensitivity, it can be advantageous for visual feedback and interactive functions in human-machine interface applications, while metallic reflective layers, with lower transmittance, provide superior precision in tactile measurements.

Please cite this article in press as: Kim et al., Modular tactile sensing platform with sequential optical sampling for human-robot interfaces, Device (2026), https://doi.org/10.1016/j.device.2026.101081

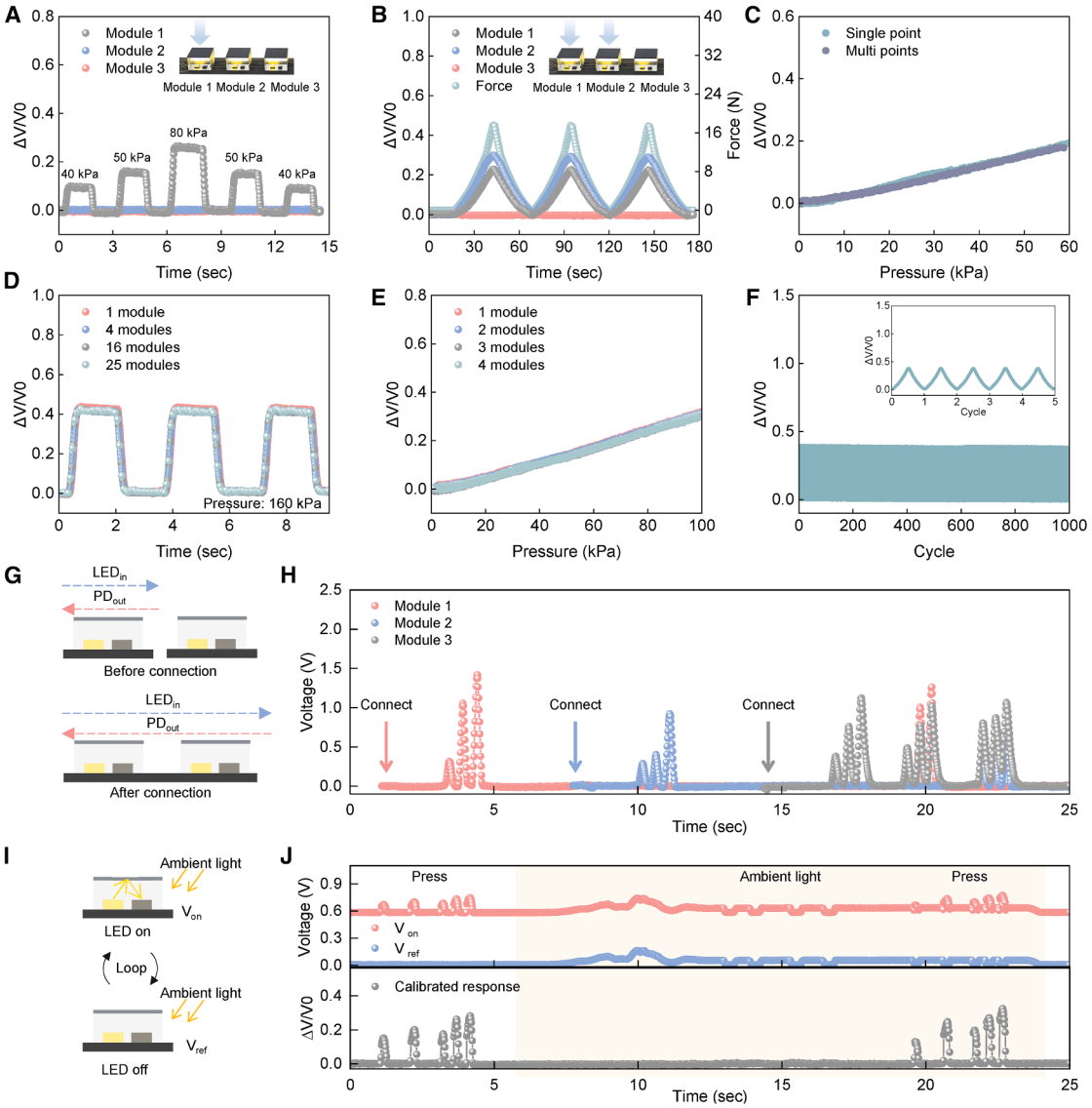

Figure 2. Characterization of the modular pressure-sensing system

(A) Time-resolved pressure response of three individual modules.
(B) Consistent multi-module response under repeated loading.
(C) Signal consistency under single and multi-point loading.
(D) Time-resolved pressure response with an increasing number of modules.
(E) Response of the pressure sensor across different module counts.
(F) Signal stability over 1,000 pressure cycles.
(G) Schematic of the plug-and-play modular connection mechanism.
(H) Real-time signal response upon sequential module connections.
(I) Schematic of ambient light calibration using LED-on and LED-off reference signals.
(J) Calibrated sensor response under alternating pressure and ambient light conditions.

Force localization with enhanced spatial resolution

To enhance spatial resolution beyond the physical limits imposed by discrete sensor spacing, a force localization sensor was developed using a continuous elastomeric medium and a spatially distributed LED-PD configuration. In conventional discrete sensor arrays,[2,4] each sensor module has a confined receptive field, meaning that force detection is spatially constrained by the physical footprint of the module itself. As illustrated in Figure 3A(i), this architecture limits spatial resolution to the sensor pitch, since each module responds only when pressure is applied directly above it. Introducing a continuous optical layer above multiple LEDs and PDs allows mechanical deformation caused by indentation to influence the optical paths across a wider area. As a result, individual LED-PD pairs exhibit

Please cite this article in press as: Kim et al., Modular tactile sensing platform with sequential optical sampling for human-robot interfaces, Device (2026), https://doi.org/10.1016/j.device.2026.101081

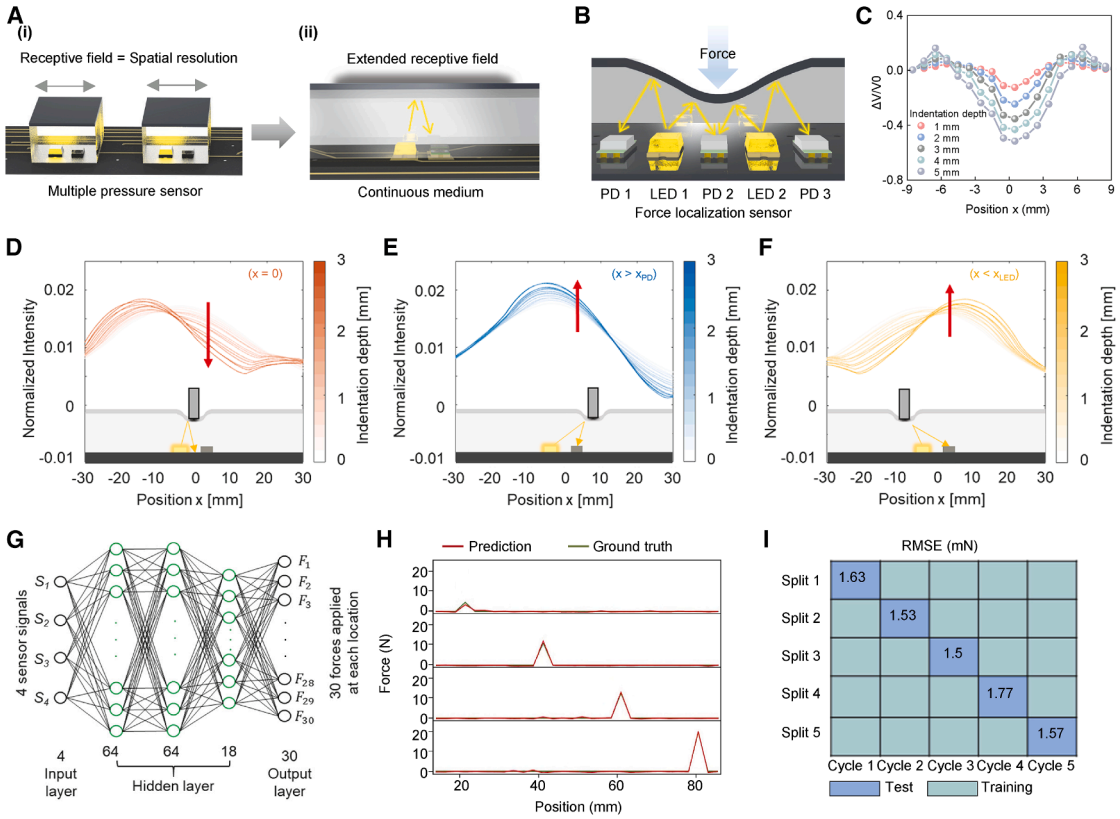

Figure 3. Force localization using a modular tactile sensor and machine learning

(A) Conceptual schematic illustrating the extended receptive field of an LED-PD pair through a continuous optical transmission medium.

(B) Schematic of the force localization sensor based on optical path changes induced by indentation.

(C) Sensor response curves for various indentation positions and depths.

(D–F) Simulated normalized intensity maps for indentation at (D) the center (x = 0), (E) the right side (x > xPD), and (F) the left side (x < xLED).

(G) Architecture of the machine learning model used for force localization.

(H) Prediction and ground-truth force profiles on the test set, showing high agreement.

(I) Root-mean-square error (RMSE) values across five data splits, each using one press-release cycle as the test set.

broadened, overlapping receptive fields (Figure 3A(ii)) so that a single indentation affects multiple sensor channels simultaneously, enabling interpolation of force position and magnitude beyond the physical sensor spacing. Alternating LEDs and PDs create overlapping receptive fields that jointly indicate force location and magnitude through differential sensitivity (Figure 3B), enabling interpolation for localization. This configuration preserves the same shift register-based control logic and sequential sampling method as described in Figures 1D and 1G while expanding the LED-PD spacing and distributing PDs across a continuous sensing surface. Although this layout departs from the modular structure introduced in Figures 1 and 2, it is introduced as a complementary architecture to demonstrate high-resolution tactile sensing based on overlapping optical fields and machine learning-assisted signal decoding.

As shown in Figure 3B, when a local indentation is applied, deformation of the reflective surface alters the light paths reaching the PDs. Depending on the indentation location, light may be redirected toward or away from the PD, resulting in a signal increase or decrease, respectively. The sensor module consisted of multiple PDs and LEDs arranged in an interleaved arrangement with 2.5 cm spacing. The sensor was fabricated by positioning the LED-PD device onto a rigid mold, followed by pouring of the prepolymer and a reflective particle mixture (Figure S10). After leveling the reflective mixture via bar coating and room-temperature curing for 3 h, the sensor was demolded to reveal a flat surface with integrated optical elements (Figure S10A). A photograph of the completed sensor is shown in Figure S10B. Before characterizing the sensor response under applied indentation, mechanical and environmental stabilities were evaluated through repeated loading and varying temperature/humidity conditions, respectively. The module withstood 200 cycles of loading and unloading under a 15 N force (6 mm indentation depth), showing minimal signal drift (Figure S11). Stable operation was also observed under varying temperature (20°C–80°C) (Figure S12A) and relative humidity (20%–80%) (Figure S12B) conditions, with negligible changes in signal output.

The output signal ($\Delta V/V_0$) was measured at various indentation positions and depths using a 15 mm cylindrical indenter and 5 mm indentation depth (Figure 3C). Spatially distinct signal

Please cite this article in press as: Kim et al., Modular tactile sensing platform with sequential optical sampling for human-robot interfaces, Device (2026), https://doi.org/10.1016/j.device.2026.101081

patterns were observed depending on whether the force was applied at the center ($x = 0$), right ($x > x_{PD}$), or left ($x < x_{LED}$) side of the sensor. The response characteristics reflect how light rays are blocked or redirected as the reflective surface deforms. These behaviors were confirmed through ray optics and mechanical simulations, showing good agreement with experimental data (Figures 3D, 3E, and S13).

To develop a force localization model, signal outputs from multiple LED-PD channels were collected at varying force magnitudes and positions. The sensor was indented at 2.5 mm intervals along the sensing area using a linear stage, and the measurement process was repeated five times to ensure sufficient training data (Figure S14). Figure S13C–S13F show the sensor responses for each PD pair as the force was incrementally increased from 0 to 20 N. The resulting intensity patterns exhibited unique gradients depending on the position and direction of deformation, enabling their use as features for machine learning-based regression. A fully connected multilayer perceptron (MLP) was implemented to predict force magnitude at enhanced spatial resolution, with four input nodes; three hidden layers containing 64, 64, and 18 units; and 30 output nodes (Figure 3G). The 4 inputs were defined as signals from LED_1-PD_1, LED_1-PD_2, LED_2-PD_2, and LED_2-PD_3. The 30 outputs were defined as indentation forces at discrete positions from x = 13.75–86.25 mm each, spaced at 2.5 mm intervals. The dataset enabled five test splits; in each case, one press-release cycle was used as the test set and the remaining four as the training set. Figure 3H visualizes the predicted force distributions for the split 1 test set, where ground-truth forces of 5, 10, 15, and 20 N were applied at positions x = 21.25, 41.25, 61.25, and 81.25 mm, respectively. Results for all position nodes are summarized in Figure S15, which compares predicted and ground-truth forces at 5, 10, and 15 N, showing improved accuracy at higher force levels. Figure 3I presents the node-averaged root-mean-square error (RMSE) across all splits, with a mean RMSE of 16.0 mN and a standard deviation of 0.955 mN. During training, the data were divided into training and validation sets at a 3:1 ratio to mitigate overfitting. Early stopping was applied with a patience of 100 epochs, and training was terminated when the validation loss no longer decreased, using the Adam optimizer. These findings demonstrate that a 10-fold enhancement in spatial resolution can be achieved over the 2.5 cm sensor-to-sensor pitch without increasing hardware complexity or sensor density. The approach preserves the compact and scalable nature of the modular platform while enabling precise, data-driven force localization through machine learning.

Modular tactile system as a human-machine interface

Leveraging the modular structure and integrated optoelectronics, the tactile sensor was adapted as a customizable human-machine interface (HMI) capable of pressure detection and visual feedback (Figure 4A). Each module uses its embedded LED to reflect pressure magnitude through color and intensity modulation, forming a closed feedback loop that enables intuitive user interaction without the need for an external graphical interface. In this system, the LED driving and PD readout are synchronized within a single microcontroller unit program. For each module (n), the LED is first activated for signal acquisition, and the PD output is sampled. The same LED is then reactivated for visual feedback according to the measured pressure, while signal sampling is disabled during the feedback illumination period. This time-sequential operation prevents optical feedback from influencing the PD response, ensuring signal fidelity. In the demonstration, six sensor modules were arranged with blue-green-red feedback colors in a repeating pattern (Figure 4B). LED intensity scaled proportionally with applied pressure and could be tuned to accommodate user-specific thresholding or color mapping preferences (Video S3). As shown in Figure 4B(i–iv), the system generated distinct visual output corresponding to both single and multi-module inputs, validating its use as a self-contained tactile interface.

Miniaturization was realized with a single sensor size of 4 × 4 mm by utilizing compact commercial components, including a 1.5 × 1.5 mm LED and a 2 × 1.5 mm PD. A 3 × 3 sensor array with 6 mm spacing was fabricated to demonstrate scalable integration with a fixed number of channels (Figure 4C(i–ii)). Each module output was normalized using its maximum pressure-induced voltage change (Figure S16), and pressure calibration was performed via polynomial fitting. Inter-sensor normalization by dividing each signal by its maximum value further reduced variability (Figure S16A). A second-order polynomial fitting yielded a strong agreement across modules (R^2 = 0.9998) (Figure S16B).

Real-time pressure mapping was achieved by assigning calibrated outputs to a 3D visualizer, which displayed both isolated and distributed pressure inputs (Figures 4D; Video S4). The array operated with a fixed number of channels and demonstrated consistent behavior across various loading scenarios. These demonstrations confirm that the proposed modular sensor platform can function as a responsive and reconfigurable HMI. The integration of sensing and feedback within each module simplifies system design and enables user-friendly interaction. The modularity and scalability of the platform provide the potential of tailoring to different surface geometries and application environments.

Robotic demonstration with a modular tactile sensor

To ensure safe and responsive physical interaction between robots and external stimuli, tactile sensors must be scalable, soft, and conformable to the robot's geometry (Figure 5A). These requirements are important for integration into articulated robotic arms used in human-robot interaction scenarios. To demonstrate this concept, a modular sensor strip was developed and integrated into a collaborative robotic arm (UR5e, Universal Robots). Each strip contains eight tactile sensor units arranged linearly and includes exposed electrodes at both ends, enabling interconnection using standard commercial connectors. The strips were fabricated on flexible printed circuit boards (FPCBs) to conform to the curved surface of the robot and arranged in an L-shaped configuration, covering both the axial side of the link and the circumferential surface of the wrist (Figures 5B and 5C). The modular structure enabled straightforward integration without altering the existing hardware layout, and power and data lines were shared across modules to minimize wiring complexity.

Please cite this article in press as: Kim et al., Modular tactile sensing platform with sequential optical sampling for human-robot interfaces, Device (2026), https://doi.org/10.1016/j.device.2026.101081

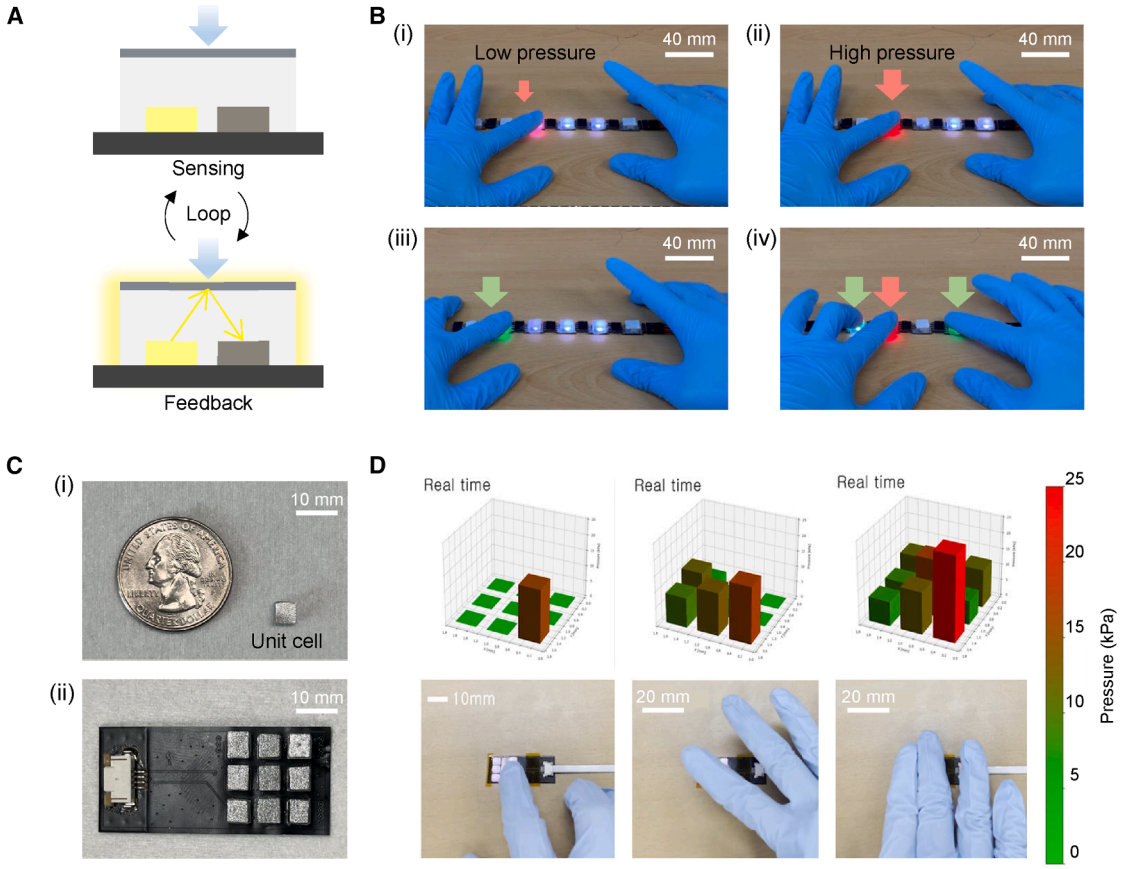

Figure 4. Real time feedback and miniaturization of the modular pressure-sensing system

(A) Schematic and demonstration of the closed-loop sensing-feedback mechanism, where each module uses its embedded LED to visualize applied pressure.

(B) Color- and intensity-coded responses of six modules arranged in a blue-green-red repeating pattern, showing distinct outputs for single and multi-module inputs.

(C) Photograph of a miniaturized 4 × 4 mm sensor unit and a 3 × 3 sensor array with 6 mm spacing.

(D) Real-time pressure mapping via 3D visualization of calibrated sensor outputs.

To evaluate real world interaction, a series of human hand gestures (finger tap, grasp, and push) were applied to the robotic arm (Figure 5D(i–v)). The system localized physical contact events in real time and displayed corresponding voltage responses and pressure profiles. A predefined voltage threshold (V_{thd}) equivalent to 100 mV was set for impact detection. When the peak signal exceeded this threshold, the robot halted its operation to prevent excessive force, as shown in Video S5.

Quantitative response profiles from the link-mounted sensor strip are presented in Figure 5E. Contact events at two time points generated distinct responses in sensors 1–8, with corresponding voltage peaks reaching up to approximately 0.4 V. Similarly, Figure 5F shows the voltage response from the wrist-mounted sensor array, where sensors 9–24 detected multiple signals throughout the 0–16 s time period in response to different contact events. Circumferentially placed sensors enabled directional detection of wrist-applied forces (Figure 5D(ii, iii, v)), while axially mounted sensors captured longitudinal contact patterns (Figure 5D(i, iv)).

Conclusion and outlook

We developed a modular tactile sensor platform that combines scalability, compact architecture, and high configurability through the SRSOS method. By decoupling sensing from wiring complexity, the system enables customizable tactile arrays using a fixed number of electrical lines.

Using the SRSOS method, the pressure sensors exhibited consistent performance across configurations, demonstrating high repeatability, and plug-and-play functionality. Ambient light effects were mitigated through LED on/off-based calibration, and sensor normalization ensured inter-module uniformity. Machine learning extended the sensing capability to high-resolution force localization, achieving a 10-fold spatial resolution enhancement without increasing physical sensor density. A key feature of the platform is its modularity at both the hardware and system levels. Plug-and-play interconnects and flexible substrates allow sensors to be rearranged, replaced, or scaled to match application-specific requirements. This was demonstrated in robotic applications, where the tactile sensor strips

Please cite this article in press as: Kim et al., Modular tactile sensing platform with sequential optical sampling for human-robot interfaces, Device (2026), https://doi.org/10.1016/j.device.2026.101081

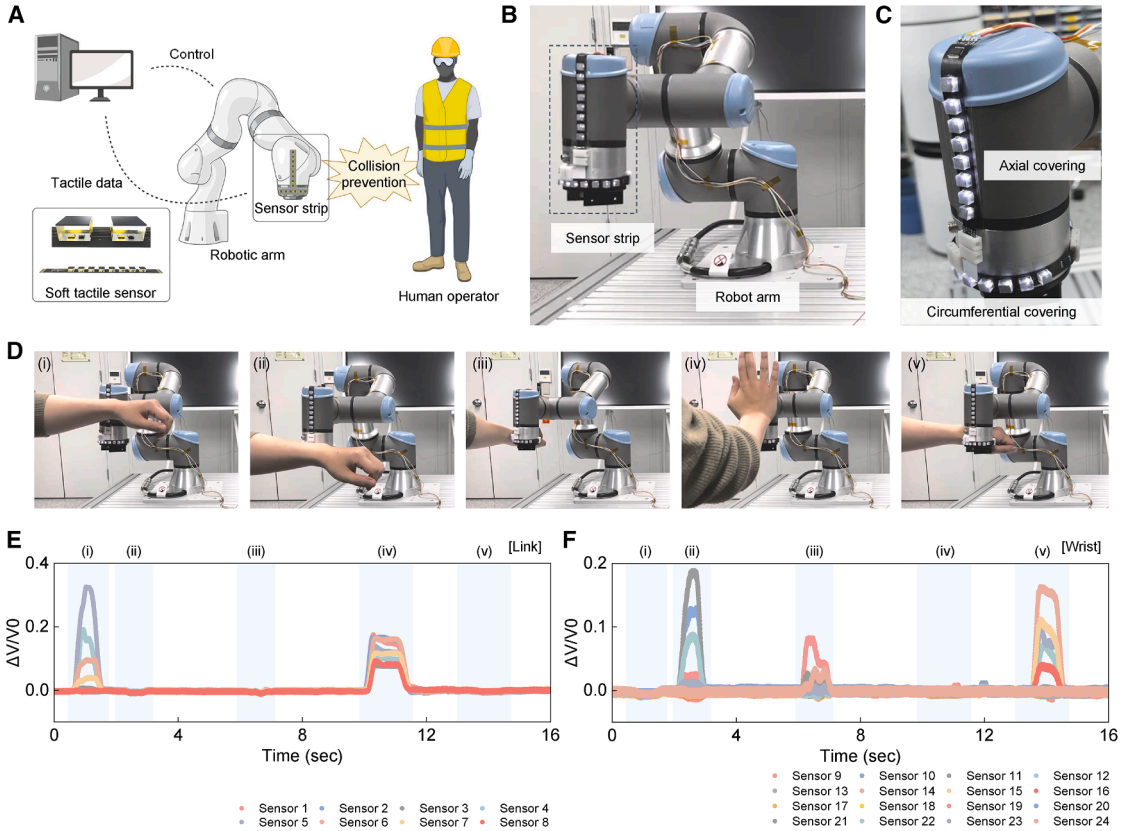

Figure 5. Robotic application of the modular tactile sensor system

(A) Schematic illustrating the use of soft, conformable, and scalable tactile sensors for human-robot interaction and collision prevention.

(B) Integration of the modular sensor strip into a robotic arm.

(C) Flexible deployment along both axial and circumferential robot surfaces in an L-shaped configuration.

(D) Demonstration of physical interaction through user hand gestures, showing localized and multi-point responses. The robot recognizes forces on multiple points on robot link (i and iv) and wrist (ii, iii, and v).

(E) Sensor response on the link-mounted sensors.

(F) Sensor response on the wrist-mounted sensors.

were mounted on the link and wrist of a collaborative robotic arm. The system identified contact events in real time and triggered safety responses based on calibrated pressure thresholds, validating its potential for physical human-robot interaction.

The system's underlying circuit architecture, control logic, and SRSOS method remain unchanged regardless of the target stimulus. This enables diverse sensing modalities to be implemented by modifying the mechanical or optical components. For example, a thermochromic reflective layer could enable temperature sensing,[17] while a customized LED-PD layout may support multi-axis force or strain detection. This decoupling between electronic architecture and sensing function highlights the platform's potential as a generalizable solution for multimodal tactile and structural sensing.

Despite these advantages, the sampling rate is inversely related to the number of connected modules, and the current response time may limit applications involving high-frequency dynamic stimuli. These limitations are primarily determined by the ADC conversion time and shift register speed and could be alleviated by employing faster readout electronics. The system is designed for normal-pressure sensing; however, it can be extended toward multi-axis tactile perception, including shear and bending responses. This can be achieved by incorporating modified mechanical and optical stack designs while maintaining the same scalable electronic architecture. Although the current robotic demonstration utilized linear strip configurations, the modular design inherently supports more complex geometries. Flexible branching, angled interconnects, or multi-plane modular assemblies can enable tactile coverage on highly contoured surfaces such as articulated joints or curved robot exteriors. Future versions of the platform may incorporate wireless communication or onboard signal processing to reduce system footprint and latency, enhancing mobility and integration in untethered applications. Systematic optimization of the LED-PD spacing and alignment could further enhance spatial resolution and improve the regression accuracy of the machine learning-based force localization.

Please cite this article in press as: Kim et al., Modular tactile sensing platform with sequential optical sampling for human-robot interfaces, Device (2026), https://doi.org/10.1016/j.device.2026.101081

METHODS

Fabrication of the optical tactile sensor

The tactile sensor was fabricated by integrating an LED and PD onto a custom-designed PCB, followed by encapsulation in a soft elastomer and application of a reflective surface. The specific component configurations varied by sensor type. For 10 × 10 mm pressure sensors and the force localization sensor, 5 × 5 mm LEDs (SK6812, NeoPixel) and 4 × 2 mm PDs (TEMT6000X01, Vishay) were used. The sensor strip utilized 2 × 1.25 mm LEDs (LS-SP172DBW91, Hsukwang) and 2 × 1.5 mm PDs (SFH2716, Osram), while the 4 × 4 mm miniaturized array used 1.5 × 1.5 mm LEDs (SK6805, NeoPixel) and 2 × 1.5 mm PDs (SFH2716, Osram). Custom molds were fabricated via a fused deposition modeling (FDM) 3D printer (Ultimaker, the Netherlands), with mold designs tailored to each sensor geometry. The elastomer (Ecoflex 00-31, Smooth-On) was mixed at a 1:1 weight ratio, degassed, poured over the mounted components, and cured at room temperature under a flat glass plate. For the reflective layer, a mixture of metallic powder and Ecoflex (10:10:1 by weight) was spin coated (for pressure sensors) or bar coated (for strips and localization sensors), followed by an additional curing step. The complete step-by-step fabrication process and resulting sensor form factors are illustrated in Figures S6A and S11A. Representative photographs of the fabricated sensors are shown in Figures S6B and S11B. Each sensing unit based on the FPCB architecture was supported by a rigid FR-4 (1 mm) backing beneath the flexible circuit layer to prevent global bending during fabrication and testing, ensuring that the optical response originated solely from vertical deformation of the elastomer.

Sensor performance characterization

The sensing characteristics were evaluated using a 10 × 10 mm module subjected to compressive loading via a universal testing machine (AGS-X, Shimadzu, Japan) equipped with a 15-mm-diameter cylindrical indenter at 0.1 mm/s. A calibrated load cell connected to a 24-bit analog-to-digital converter (HX711, Avia Semiconductor) measured the applied force, while a custom MCU was used to acquire the sensor voltage output. To investigate the sensor response (ΔV/V0) under different conditions, three sensor modules were connected in series. For both single-module and multi-module loading conditions, pressure was applied to only the target sensor by adjusting the indenter size to match the sensing area of the intended module.

Mechanical and optical simulation

To analyze how mechanical deformation influences optical signal transmission, finite element analysis (FEA) and ray optics simulations were performed sequentially. Mechanical simulations were performed using Abaqus software (Dassault Systèmes Simulia, Johnston, RI, USA). To model the deformation of the elastomer (Ecoflex 00-31, Smooth-On), the Yeoh hyperelastic model was applied. Material parameters were experimentally obtained and set to $C_1 = 0.0175$ and $C_2 = -0.0006$. The sensor geometry used in the simulation was identical to that of the actual force localization sensor. Automated simulations were conducted via Python scripting, and the resulting profiles of the deformed reflective surface were exported according to indentation depth and location.

Based on the simulated reflective surface profiles, optical simulations were carried out using the Geometrical Optics module in COMSOL Multiphysics 5.6. The simulation was automated using scripting to extract the ray intensity reaching the PD. Considering that the LED chip used has a planar packaging structure, the emission intensity decreases as the radiation angle increases by the refraction at the interface of package and the air. Accordingly, the LED was modeled as a point source embedded in a medium with a refractive index of 1.5. The reflective surface was assumed to be specular, with rays propagating through a vacuum and terminating upon contact with the ground.

To quantify the ray distribution at the ground surface, the spatial coordinates of scattered rays were extracted. An intensity distribution was then calculated from the discrete ray coordinates using the Epanechnikov quadratic kernel method, with a kernel size of 20 mm.

Human-interactive robotic skin

Two sensor strips were interconnected in an L-shaped configuration using a custom-designed curved connector and mounted onto a collaborative robotic arm (UR5e, Universal Robots). One strip was attached along the axial direction of the arm link and the other along the circumferential direction around the wrist joint. Each sensor strip was interfaced with a custom-built measurement circuit consisting of a microcontroller board (Teensy 4.1, PJRC) with onboard central processing unit (CPU), ADC, and general purpose input/output (GPIO) and connected to a TIA, configured with an operational amplifier (LMP7721, Texas Instruments) and a 10 MΩ feedback resistor. The robot was programmed to perform a repeated bidirectional sweeping motion (forward, backward, and lateral). A predefined threshold of 0.1 mV was implemented so that motion automatically stopped when the measured peak pressure exceeded this value and resumed when the pressure dropped below the threshold. This experiment was approved by the institutional review board of the Electronics and Telecommunications Research Institute (ETRI; 2025-HR-0012).

RESOURCE AVAILABILITY

Lead contact

Requests for further information and resources should be directed to and will be fulfilled by the lead contact, Inkyu Park (inkyu@kaist.ac.kr).

Materials availability

This study did not generate new unique reagents.

Data and code availability

The code used for training and evaluation of the deep learning model in this study is publicly available at Zenodo (https://doi.org/10.5281/zenodo.18104932).

ACKNOWLEDGMENTS

H.K., S.C., and I.P. are supported by the Technology Innovation Program (00144157, Development of Heterogeneous Multi-Sensor Micro-System Platform) funded by the Ministry of Trade, Industry and Energy (MOTIE, Korea), and the InnoCORE program of the Ministry of Science and ICT (N10250154).

J.C. is supported by an internal fund/grant from the Electronics and Telecommunications Research Institute (ETRI) (25YB2610, Thermoforming based Sensor and Actuator System for Wearable and Robotic Applications).

AUTHOR CONTRIBUTIONS

H.K., S.C., J.C., and I.P. led the development of the concepts, designed the experiments, and interpreted results. H.K. led the experimental work with support from C.H., Jihyeon Ahn, D.L., S.J., G.L., K.L., H.H., J.-H.H., Junseong Ahn, and Y.J.. H.K., S.C., J.C., and I.P. wrote the paper.

DECLARATION OF INTERESTS

H.K., J.C., and I.P. are inventors on the following patent applications related to the tactile sensor module described in this work: Korean Patent Application No. 10-2023-0035053, March 17, 2023, and PCT Patent Application No. PCT/KR2024/002986, March 8, 2024.

DECLARATION OF GENERATIVE AI AND AI-ASSISTED TECHNOLOGIES IN THE WRITING PROCESS

During the preparation of this work, the authors used ChatGPT for language editing. After using this tool, the authors reviewed and edited the content as needed and take full responsibility for the content of the publication.

SUPPLEMENTAL INFORMATION

Supplemental information can be found online at https://doi.org/10.1016/j.device.2026.101081.

Received: September 17, 2025
Revised: December 15, 2025
Accepted: February 5, 2026

REFERENCES

1. Han, C., Choi, J., Ahn, J., Kim, H., Ha, J.-H., Han, H., Cho, S., Jeong, Y., Gu, J., and Park, I. (2023). Spike-based Self-Calibration for Enhanced Accuracy in Self-powered Pressure Sensing. Adv. Mater. Technol. *8*, 2301199. https://doi.org/10.1002/admt.202301199.
2. Kong, D., Lu, Y., Zhou, S., Wang, M., Pang, G., Wang, B., Chen, L., Huang, X., Lyu, H., Xu, K., and Yang, G. (2025). Super-resolution tactile sensor arrays with sparse units enabled by deep learning. Sci. Adv. *11*, eadv2124. https://doi.org/10.1126/sciadv.adv2124.
3. Jin, J., Wang, S., Zhang, Z., Mei, D., and Wang, Y. (2023). Progress on flexible tactile sensors in robotic applications on objects properties recognition, manipulation and human-machine interactions. Soft Sci. *3*, 8. https://doi.org/10.20517/ss.2022.34.
4. Zhou, S., Kong, D., Wang, M., Wang, B., Lu, Y., Lyu, H., Lu, Z., Tao, Y., Xu, K., and Yang, G. (2025). Unlocking dynamic subtle stimuli tactile perception: a deep learning-enhanced super-resolution tactile sensor array with rapid response. Adv. Intell. Syst. *7*, 2400913. https://doi.org/10.1002/aisy.202400913.
5. Kim, J., Kim, J., and Park, Y.-L. (2024). Multi-modal modular textile sensor for physical human–robot interaction using band-stop filters. Adv. Funct. Mater. *34*, 2308571. https://doi.org/10.1002/adfm.202308571.
6. Park, H., Park, K., Mo, S., and Kim, J. (2021). Deep neural network based electrical impedance tomographic sensing methodology for large-area robotic tactile sensing. IEEE Trans. Robot. *37*, 1570–1583. https://doi.org/10.1109/TRO.2021.3060342.
7. Kim, J., Kim, S., and Park, Y.-L. (2022). Single-input single-output multi-touch soft sensor systems using band-pass filters. npj Flex Electron *6*, 65. https://doi.org/10.1038/s41528-022-00201-8.
8. Choi, J., Han, C., Cho, S., Kim, K., Ahn, J., Del Orbe, D., Cho, I., Zhao, Z.-J., Oh, Y.S., Hong, H., et al. (2021). Customizable, conformal, and stretchable 3D electronics via predistorted pattern generation and thermoforming. Sci. Adv. *7*, eabj0694. https://doi.org/10.1126/sciadv.abj0694.
9. Lee, W.W., Tan, Y.J., Yao, H., Li, S., See, H.H., Hon, M., Ng, K.A., Xiong, B., Ho, J.S., and Tee, B.C.K. (2019). A neuro-inspired artificial peripheral nervous system for scalable electronic skins. Sci. Robot. *4*, eaax2198. https://doi.org/10.1126/scirobotics.aax2198.
10. Dementyev, A., Kao, H.-L. (Cindy), and Paradiso, J.A. (2015). SensorTape: modular and programmable 3D-aware dense sensor network on a tape. In Proceedings of the 28th Annual ACM Symposium on User Interface Software & Technology UIST '15 (Association for Computing Machinery), pp. 649–658. https://doi.org/10.1145/2807442.2807507.
11. Jung, Y.H., Yoo, J.-Y., Vázquez-Guardado, A., Kim, J.-H., Kim, J.-T., Luan, H., Park, M., Lim, J., Shin, H.-S., Su, C.-J., et al. (2022). A wireless haptic interface for programmable patterns of touch across large areas of the skin. Nat. Electron. *5*, 374–385. https://doi.org/10.1038/s41928-022-00765-3.
12. Liu, S.-Z., Guo, W.-T., Chen, H., Yin, Z.-X., Tang, X.-G., and Sun, Q.-J. (2024). Recent progress on flexible self-powered tactile sensing platforms for health monitoring and robotics. Small *20*, 2405520. https://doi.org/10.1002/smll.202405520.
13. Kim, T., Kim, J., You, I., Oh, J., Kim, S.-P., and Jeong, U. (2022). Dynamic tactility by position-encoded spike spectrum. Sci. Robot. *7*, eabl5761. https://doi.org/10.1126/scirobotics.abl5761.
14. Han, S., Kim, T., Kim, D., Park, Y.-L., and Jo, S. (2018). Use of Deep Learning for Characterization of Microfluidic Soft Sensors. IEEE Robot. Autom. Lett. *3*, 873–880. https://doi.org/10.1109/LRA.2018.2792684.
15. Williams, Marshall. "Shift register delay circuit." U.S. Patent No. 4,530,107. 16 Jul. 1985.
16. Horowitz, P., Hill, W., and Robinson, I. (1989). The Art of Electronics (Cambridge: Cambridge university press).
17. Barreiros, J.A., Xu, A., Pugach, S., Iyengar, N., Troxell, G., Cornwell, A., Hong, S., Selman, B., and Shepherd, R.F. (2022). Haptic perception using optoelectronic robotic flesh for embodied artificially intelligent agents. Sci. Robot. *7*, eabi6745. https://doi.org/10.1126/scirobotics.abi6745.